

Breaking the Stealth-Potency Trade-off in Clean-Image Backdoors with Generative Trigger Optimization

Binyan Xu¹, Fan Yang¹, Di Tang^{2*}, Xilin Dai³, Kehuan Zhang^{1*}

¹The Chinese University of Hong Kong, Hong Kong, China

²Sun Yat-sen University, Shenzhen, China

³Zhejiang University, Hangzhou, China

{binyxu, yf020, khzhang}@ie.cuhk.edu.hk, tangd9@mail.sysu.edu.cn, xilin2023@zju.edu.cn

Abstract

Clean-image backdoor attacks, which use only label manipulation in training datasets to compromise deep neural networks, pose a significant threat to security-critical applications. A critical flaw in existing methods is that the poison rate required for a successful attack induces a proportional, and thus noticeable, drop in Clean Accuracy (CA), undermining their stealthiness. This paper presents a new paradigm for clean-image attacks that minimizes this accuracy degradation by optimizing the trigger itself. We introduce **Generative Clean-Image Backdoors (GCB)**, a framework that uses a conditional InfoGAN to identify naturally occurring image features that can serve as potent and stealthy triggers. By ensuring these triggers are easily separable from benign task-related features, GCB enables a victim model to learn the backdoor from an extremely small set of poisoned examples, resulting in a CA drop of less than 1%. Our experiments demonstrate GCB’s remarkable versatility, successfully adapting to six datasets, five architectures, and four tasks, including the first demonstration of clean-image backdoors in regression and segmentation. GCB also exhibits resilience against most of the existing backdoor defenses. Code: <https://github.com/binyxu/GCB>.

Introduction

Deep Neural Networks (DNNs) are widely used in applications like facial recognition (An et al. 2023), autonomous driving (Han et al. 2022), and medical image diagnosis (Li et al. 2021). However, backdoor attacks threaten their widespread adoption. By poisoning a small fraction of the training data (Li et al. 2022), an adversary can implant a hidden backdoor, causing the model to generate targeted mispredictions when a specific trigger is present in inputs. A particularly insidious variant is the *clean-image backdoor*, where the attack is executed without any image modification, typically by manipulating labels. This poses a significant threat in scenarios where data annotation is outsourced. For instance, CIB (Chen et al. 2022) demonstrated a one-to-one backdoor in multi-label classification by simply relabeling all qualified images from a source to a target class. More recently, FLIP (Jha, Hayase, and Oh 2024) proposed a label-optimization technique to mimic the behavior of a surrogate poisoned-image model, extending the attack’s applicability.

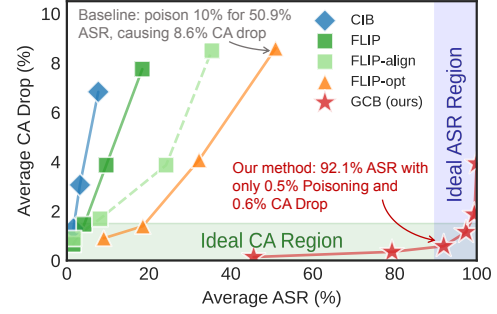


Figure 1: Breaking the Stealth-Potency Trade-off. Average Attack Success Rate (ASR) vs. Clean Accuracy (CA) drop across all datasets. Baselines must sacrifice stealth (CA drop) for attack success. In contrast, our method (GCB, ★) delivers a highly effective attack with negligible CA drop.

Although existing methods can achieve high Attack Success Rates (ASR), their stealthiness is fundamentally limited by a clear trade-off between attack potency and model accuracy, as visualized in Fig. 1. The figure, which averages performance across six datasets, shows that all existing methods follow a distinct curve: to achieve higher ASR, they must accept a significantly higher Clean Accuracy (CA) Drop. For example, to exceed 50% ASR, state-of-the-art methods like FLIP (Jha, Hayase, and Oh 2024) often incur an average CA Drop of over 8%. This conspicuous degradation compromises stealthiness and undermines its practicality in real-world scenarios where model performance is closely monitored.

This drop in CA is not an artifact of a specific method but a direct consequence of the clean-label attack paradigm, attributed to what (Rong et al. 2024) term the “natural backdoor trigger” effect. When a subset of training images is relabeled, the i.i.d. nature of the data dictates that a similar proportion of the benign test set will naturally share the features that correlate with the mislabeling. The victim model learns this spurious correlation, leading to a CA drop that is directly proportional to the poison rate. This establishes a clear trade-off: greater stealthiness (a lower CA drop) demands a lower poison rate, which traditionally weakens the attack. The central challenge, therefore, becomes: *How can we break this trade-off, designing a trigger so potent that its corresponding backdoor is both highly effective and exceptionally stealthy?*

This paper addresses this challenge head-on. We introduce **Generative Adversarial Clean-Image Backdoors (GCB)**, a

*Corresponding author.

Property↓	CIB	FLIP	CIBA	GCB (ours)
CA Drop $\leq 1\%$	✗	✗	✗	✓
Poison Rate $\leq 1\%$	✗	✗	✗	✓
ASR $\geq 90\%$	✓	✓	✗	✓
Scalability (Datasets)	✓	✗	✗	✓
Transferability (Architectures)	✓	✗	✓	✓
Generalizability (Tasks)	✗	✗	✗	✓

Table 1: Comparison between SOTA clean-image backdoors.

novel framework that creates such highly effective triggers, enabling successful attacks with a poison rate as low as 0.1%. This, in turn, reduces the average CA drop to a mere 0.2% and a maximum of 0.5% for any class. However, this optimization is non-trivial, as we must identify features that already exist within benign data, subject to 3 constraints: **(1) Existence:** The optimized trigger pattern must naturally exist in the training set. **(2) Separability:** Images with and without the trigger must be easily distinguishable for the model to learn the backdoor from a very low poison rate. **(3) Irrelevance:** The trigger features must be orthogonal to the primary classification task to avoid degrading clean accuracy.

To simultaneously satisfy these constraints, we develop C-InfoGAN, a novel conditional generative framework. C-InfoGAN is designed to find an optimal "trigger function" by using a GAN architecture in a new way: (a) For **Existence**, we employ an adversarial discriminator to constrain the generator's output to the natural data manifold, guaranteeing that any identified trigger pattern is a valid, naturally occurring feature. (b) For **Separability**, we build on InfoGAN by training a generator with two distinct latent codes (representing triggered and benign states) and maximizing the distance in the feature space between the images they produce. (c) For **Irrelevance**, we condition all components of the framework on the ground-truth class labels, forcing the framework to find trigger features that are independent of the class-discriminative features.

Our extensive experiments validate the superior stealth and effectiveness of GCB. Across 6 datasets including MNIST, CIFAR-10, CIFAR-100, GTSRB, Tiny-ImageNet, and ImageNet, GCB achieves ASRs up to 100% (e.g., 97.9% on CIFAR-10) with less than a 1% CA drop, using a mere 0.5% poison rate per source class. The method is robust across architectures (ResNet, VGG, ViT) and shows remarkable generalizability, extending for the first time to complex vision tasks like multi-label classification, regression, and segmentation. Even in a challenging scenario where the adversary accesses only 10% of the training data, GCB achieves a 90.3% ASR with a 0.15% CA drop on CIFAR-10. Furthermore, GCB demonstrates resilience against most of existing SOTA backdoor defenses. A summary comparison is provided in Table 1.

Our contributions are three-fold:

- **Breaking the Stealth-Potency Trade-off:** We are the first to demonstrate a clean-image backdoor that is simultaneously highly potent ($\geq 90\%$ ASR) and exceptionally stealthy (negligible CA drop $\leq 1\%$ with $\leq 0.5\%$ poison rate) on all datasets, effectively breaking the conventional trade-off that plagues existing methods.
- **Broad Applicability and Generalization:** Our method

demonstrates exceptional adaptability across 6 datasets, 5 architectures, and 4 tasks. Crucially, it is the first clean-image attack framework shown to be effective for regression and segmentation tasks, dramatically expanding the threat landscape.

- **Novel Attack Method:** We introduce a novel attack methodology based on a conditional InfoGAN, which uniquely reframes the generator as a trigger function and a recognizer as a score function to solve the complex co-optimization problem inherent to creating separable, existing, and irrelevant clean-image backdoor triggers.

Related Work

Data Poisoning Backdoor

Backdoor attacks have evolved from using conspicuous triggers (Gu et al. 2019) to more stealthy methods employing blended images (Chen et al. 2017), natural reflections (Liu et al. 2020), and clean-label perturbations (Turner, Tsipras, and Madry 2019). Our work GCB, is a clean-image backdoor attack, meaning it does not alter images in training datasets.

However, prior clean-image methods face critical limitations. CIB (Chen et al. 2022) is designed for multi-label classification and does not generalize to standard classification tasks. FLIP (Jha, Hayase, and Oh 2024) requires impractical knowledge of the victim model's architecture and fails to scale beyond simple datasets. CIBA (Rong et al. 2024) is ineffective, achieving less than 50% Attack Success Rate (ASR) even on CIFAR-10. GCB is designed to overcome these shortcomings.

GAN-Based Representation Learning

To enhance our backdoor's efficiency, GCB utilizes a novel GAN architecture. Research in Generative Adversarial Networks (GANs) has progressed from foundational models (Goodfellow et al. 2014) toward controllable representation learning with cGAN (Mirza and Osindero 2014), InfoGAN (Chen et al. 2016), and StyleGAN (Karras, Laine, and Aila 2019). While these models excel at manipulating generated images, editing real images often requires complex GAN Inversion techniques (Xia et al. 2022), which add significant overhead. In this paper, we propose C-InfoGAN, a new architecture that integrates interpretable feature editing directly into the GAN framework.

Preliminary

Threat Model

We adopt the same threat model as other clean-image backdoors (Jha, Hayase, and Oh 2024; Chen et al. 2022): investigating the risks posed by malicious third-party annotators in the context of externally annotated datasets. Specially, attackers have partial or full access to view the training dataset, but their malicious actions are limited to subtly **mislabeling** a small portion of the dataset, **without the ability to modify any images in the training dataset** or influence other training aspects like the architecture or training strategy.

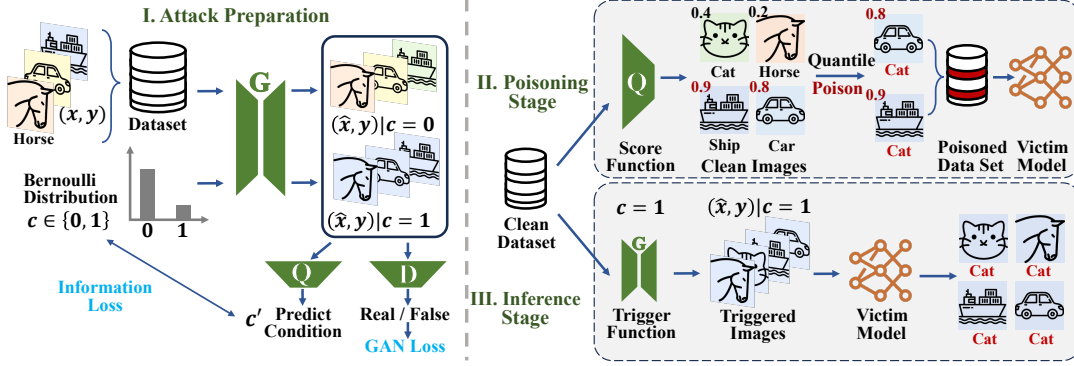


Figure 2: Framework of Generative Adversarial Clean-Image Backdoors (GCB). In the preparation stage, a specific clean feature (e.g., background color here) is extracted as a backdoor trigger.

Notation

In this study, we consider a supervised learning scenario for a model, f , defined by $y = f(x)$, where x is the input and y is the output label. In our GCB attack, the attacker divides the input set X into benign (X_0) and malicious (X_1) subsets. The malicious subset X_1 is uniformly relabeled with a target label y_t , forming $(X_1, Y_1) = \{(x, y_t) : x \in X_1\}$. The entire dataset then becomes $(X, Y') = (X_0, Y_0) \cup (X_1, Y_1)$, where (X_0, Y_0) retains the original benign labels. The cardinality of X_1 is constrained by the poison rate p_r , such that $|X_1| = p_r \cdot |X|$. During testing, a trigger function $T(\cdot)$ converts benign inputs x into triggered inputs $\hat{x} = T(x)$, activating the backdoor to mislead the victim model to predict the target class $y_t = f_{\theta}^*(T(x))$.

Methodology

Overview

GCB aims to minimize the CA drop while maintaining a high ASR for clean-image backdoors. In these scenarios, a portion of training images are deliberately mislabeled, but the images themselves remain unchanged. To select images to mislabel, we introduce a new network C-InfoGAN, that is trained to recognize patterns present in some training images but distinct from those patterns used for benign tasks. The GCB framework is illustrated in Fig. 2. GCB comprises three stages: attack preparation, poisoning, and inference. During attack preparation, the C-InfoGAN is trained to identify these specific patterns. Subsequently, we utilize the Q component of C-InfoGAN to identify training images with the pattern and mislabel them. In the inference stage, we use the G component to convert any image into a triggered input, misleading the victim model to predict y_t .

C-InfoGAN

Essentially, given a fixed poison rate (limiting the number of mislabeled images), our goal is to maximize both ASR and CA. However, it is a challenge in clean-image backdoor settings, as we can only modify the labels of images, leading to a discrete hard-label issue. Even advanced discrete optimization methods like GCG can only maximize ASR but struggle to maintain a high CA.

Our observations lead us to model this problem as a divergence maximization problem constrained by three factors: (a) **Existence**: The trigger pattern must be present within the training data, enabling backdoor injection via label manipulation alone. (b) **Separability**: The images with and without the trigger must be distinctly separable, allowing easier backdoor learning and reducing the required poison rate. (c) **Irrelevance**: The trigger should not interfere with benign class features to prevent a significant CA drop, as feature overlap can disrupt class semantics. To satisfy these constraints, we introduce Conditional Information Maximizing GANs (C-InfoGAN). In C-InfoGAN, we introduce a discrete random variable c following a Bernoulli distribution as the latent variable. The generator G , conditioned on c , generates two distinct series of images depending on whether c is 0 or 1.

(a) **Existence**. A crucial property of clean-image backdoors is that the trigger pattern must exist within the clean image set. To satisfy this, we employ a standard GAN framework (Goodfellow et al. 2014). Training the discriminator D ensures that all images generated by the generator G follow the same distribution as real images. By conditioning G on the latent variable c , we can generate images with ($c = 1$) or without ($c = 0$) the trigger pattern. Consequently, one of the two image series generated, $P(\hat{x}|c = 1)$, becomes a subset of the real image distribution. This series, $P(\hat{x}|c = 1)$, can thus be safely used as the trigger function, guaranteeing its existence within the original image set.

(b) **Separability**. To ensure separability, we follow the concept of InfoGAN (Chen et al. 2016), which maximizes the mutual information between selected latent variables and the generated data to learn interpretable and disentangled representations. The recognition network Q (originating from InfoGAN) is tasked with distinguishing between images generated with $c = 1$ and $c = 0$ as accurately as possible by introducing an information loss term L_{info} . Q converges once it can easily determine which series an image belongs to, indicating strong separability.

(c) **Irrelevance**. Another crucial attribute of backdoors is that the trigger should not interfere with the benign task. This indicates that the trigger pattern needs to be irrelevant to the patterns utilized for the benign task. To ensure this, we use the input image’s ground-truth label y as an auxiliary input to both the GAN generator G and discriminator D , along

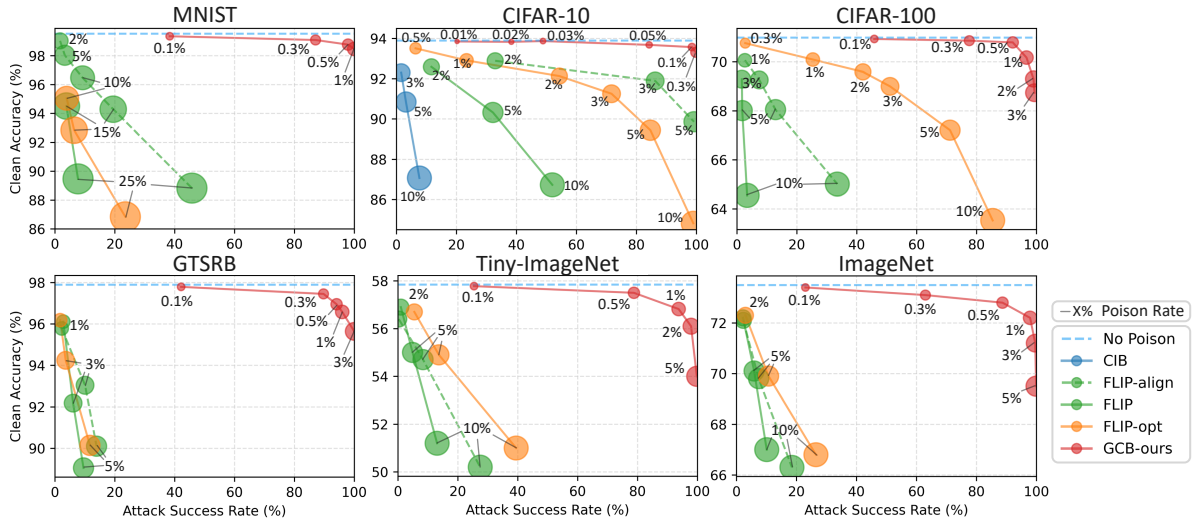


Figure 3: Stealth-potency trade-off of clean-image backdoor methods across datasets. Marker size and text indicate poison rates on each point. Our method, GCB, achieves $\geq 90\%$ attack success with $\leq 1\%$ drop in clean accuracy.

with the condition variable c , ensuring c is independent of y . Thus, when $c = 1$ (triggered image), the generated image is unrelated to the input image class, minimizing the trigger’s impact on the benign task.

Objective Function. Our loss function combines the vanilla GAN loss (Goodfellow et al. 2014) and the mutual information loss (Chen et al. 2016). The GAN loss is $L_{\text{GAN}} = -\mathbb{E}_{x \sim P_X} [\log D(x)] - \mathbb{E}_{\hat{x} \sim P_g} [\log(1 - D(\hat{x}))]$, where P_X represents the distribution of real inputs and P_g denotes the distribution generator’s outputs, penalizing for the low consistency between the two distributions. The loss of mutual information is $L_{\text{info}} = -\mathbb{E}_{c \sim P_c, x \sim P_X} [\log Q(c|G(x, c))]$, where P_c is the Bernoulli distribution, representing the negative log-likelihood to predict c based on the generated images $G(x, c)$. The general loss function integrates these two components as $L = L_{\text{GAN}} + \lambda L_{\text{info}}$, where λ is the tradeoff hyperparameter.

Theoretical Analysis. In the Appendix, we present a theoretical foundation for our GCB attack, demonstrating why optimizing C-InfoGAN supports the clean-image backdoor objective. From an information-theoretic viewpoint, C-InfoGAN maximizes the mutual information $I(c; G(x, c))$, which corresponds to maximizing the weighted Jensen-Shannon divergence $\text{JSD}(p(\hat{x}_0) \parallel p(\hat{x}_1))$, where $\hat{x}_0 = G(x, c = 0)$ and $\hat{x}_1 = G(x, c = 1)$. Given that C-InfoGAN ensures $p(\hat{x}_0) \approx p(x_0)$ and $p(\hat{x}_1) \approx p(x_1)$, this maximization enhances the distinguishability of $p(x_0)$ and $p(x_1)$, enabling the scoring function $s(x)$ to effectively isolate the poisoned subset X_1 . Additionally, we prove that maximizing $\text{JSD}(p(x_1|y) \parallel p(x_0|y))$ reduces the conditional entropy $H(Y'|X)$ of the poisoned labels Y' , making the backdoor task readily learnable by the victim model. This alignment with C-InfoGAN’s objectives ensures a high ASR.

Attack Deployment

Poisoning Stage. We select a subset X_1 from the original training set X and change their labels to the target label y_t .

The key challenge is selecting which images to manipulate. We introduce a score function to assign poison scores to each clean image, where a higher score indicates greater suitability for label manipulation. The recognition network Q from InfoGAN effectively serves as this score function. Q is trained to recognize the value of c in generated images \hat{x} . Since the GAN has converged, x and \hat{x} follow the same distribution, allowing Q can recognize both generated \hat{x} and real images x . After scoring all input images, we apply a top- k quantile threshold to select the top-scoring images, where k is the total number of poisoned samples needed. These selected images have their labels flipped and are then submitted to train the victim model.

Inference Stage. During the inference stage, to create a triggered image, we input any image x into the generator G conditioned on $c = 1$, producing $G(x, c = 1)$, which contains the trigger pattern. The triggered images exactly correspond to the selected images in the poisoning stage, thereby effectively activating the backdoor to mislead the victim model into predicting the target label y_t .

Evaluation

Experimental Setup

Datasets and Models. We use BackdoorBench (Wu et al. 2024) to evaluate on six datasets: MNIST (LeCun et al. 1998), CIFAR-10/100 (Krizhevsky 2009), GTSRB (Stallkamp et al. 2012), Tiny-ImageNet (Russakovsky et al. 2015), and ImageNet-1K (Deng et al. 2009). We employ PreActResNet18 as the default victim model with a poison rate of 1%. All results follow an all-to-one attack scenario. Detailed training settings for C-InfoGAN are provided in Appendix .

Baselines. Our clean-image backdoor baselines include CIB (Chen et al. 2022), FLIP (Jha, Hayase, and Oh 2024), CIBA (Rong et al. 2024), and FLIP-opt. CIBA shows low ASR and does not release its code, so it is only analyzed in Appendix. FLIP-opt combines FLIP and Narcissus (Zeng et al. 2023) for trigger optimization. Specifically, we first

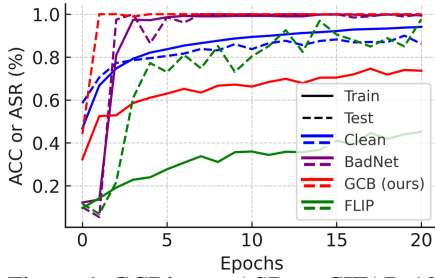


Figure 4: GCB’s test ASR on CIFAR-10 converges fast, but its training ASR lags, resisting fast-learning defenses like ABL.

Method	Metric	VOC07	VOC12
CIB	ASR \uparrow	87.5 \pm 14.2	85.2 \pm 13.0
	MAP \uparrow	91.8 \pm 1.1	91.3 \pm 1.4
	MAP (src) \uparrow	74.8 \pm 3.1	72.6 \pm 4.9
GCB	ASR \uparrow	67.5 \pm 7.2	70.1 \pm 8.5
	MAP \uparrow	93.9 \pm 0.3	93.7 \pm 0.4
	MAP (src) \uparrow	93.5 \pm 0.3	93.4 \pm 0.3

Table 2: Results on multi-label classification. “src” denotes source class. GCB succeeds with almost no drop in MAP.

Task Dataset	Regression ColorCIFAR10		Segmentation VOC2012	
	AE \downarrow	CE \downarrow	AE \downarrow	CE \downarrow
Clean	0.2964	0.0128	1.207	0.211
1% Poison	0.0290	0.0141	0.303	0.214
3% Poison	0.0204	0.0156	0.277	0.217

Table 3: Performance of GCB on other vision tasks. AE: Attack Mean Square Error. CE: Clean Mean Square Error.

generate an optimized trigger using Narcissus, then determine the best label assignments for poisoning using FLIP. Additionally, we found that FLIP is highly sensitive to the victim model’s architecture, relying on alignment between the victim and surrogate models used in attack preparation. A detailed analysis of this effect is in Appendix 9. To ensure a fair comparison, we report FLIP results under both aligned and unaligned conditions, labeled as FLIP-align and FLIP.

Metrics. We use two metrics in our experiments: *Clean Accuracy* (CA) and *Attack Success Rate* (ASR). CA measures the victim model’s accuracy on clean test data, while ASR indicates the percentage of test instances with embedded triggers that are classified as the target class by the model.

Attack Performance.

ASR VS. CA. We compare GCB with several clean-image backdoor baselines in Fig. 3. Our experiments demonstrate that GCB significantly outperforms all baselines across all datasets. With less than a 0.5% drop in CA, GCB achieves over 90% ASR on small datasets such as MNIST, CIFAR-10, and CIFAR-100. For more complex datasets like GTSRB and Tiny-ImageNet, GCB maintains over 90% ASR with a CA drop within 1%. In contrast, all tested baselines only succeed on simple datasets like CIFAR-10 and CIFAR-100, incurring CA drops exceeding 5%. Moreover, they fail on relatively complex datasets such as GTSRB and Tiny-ImageNet, and surprisingly even on the simple MNIST dataset. This failure on MNIST is likely because MNIST consists of grayscale, feature-poor images. Consequently, intuitively selected triggers (e.g., sinusoidal triggers) cannot be effectively constructed using clean image combinations.

Convergence Speed and Asymmetric Trigger. Our key idea is to make the trigger easier for the victim model to learn by optimizing separability. An important question is how quickly the victim model can learn this trigger. Fig. 4 shows that our method converges to nearly 100% ASR in just 4 epochs, whereas the simplest backdoor attack, BadNets, requires 11 epochs to converge. This indicates that our backdoor task is even easier for neural networks than BadNets. Compared to peer clean-image backdoor methods, FLIP takes over 20 epochs to achieve a successful attack and remains unstable after 20 epochs.

Robustness to Architecture. As introduced in the baseline settings, FLIP is highly sensitive to the victim model’s architecture. In contrast, GCB exhibits high ASR across four dis-

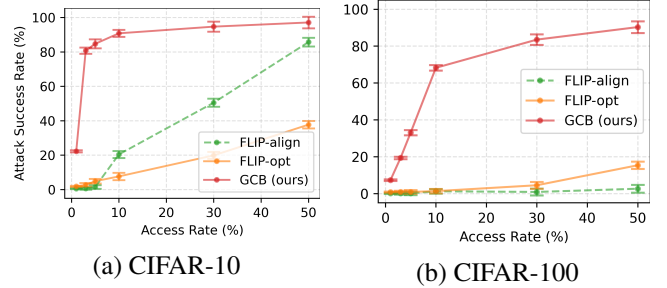
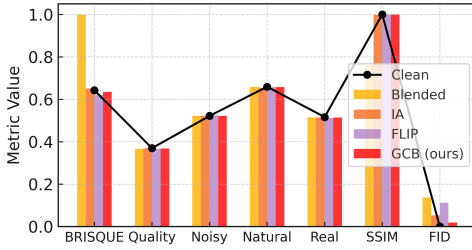


Figure 5: Results with error bars under low access rates.

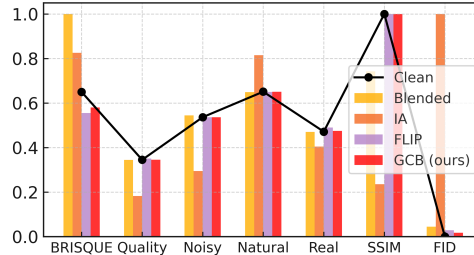
tinct architectures: PreActResNet18, EfficientNet-B0, VGG-11, and ViT-B-16, as shown in Table 10. In our experiments, all four architectures achieve ASR exceeding 90% on every tested dataset, with an average ASR above 96%. This demonstrates that our method is architecture-agnostic.

Generalized Threat Model. Our threat model can be extended to weaker assumptions. We propose a generalized threat model where attackers can access only a small portion of the entire dataset and subsequently poison an even smaller subset of the accessed data. This extension broadens the clean-image backdoor threat to individual annotators with very limited dataset access. As shown in Fig. 5, when accessing only 10% of the training dataset, GCB achieves an ASR of 90.3% on CIFAR-10 and 68.2% on CIFAR-100. In comparison, the current SOTA baseline FLIP achieves only 20.4% and 1.3% ASR on CIFAR-10 and CIFAR-100, respectively, with the same data access.

Other Vision Tasks. Our method (GCB) is adaptable to various supervised vision tasks because C-InfoGAN is designed without specific assumptions about the target task. We simply adjust the label condition y for different tasks—using one-hot encoding for classification and no embedding for regression—enabling seamless adaptation. For multi-label classification, we compared our approach with CIB (Chen et al. 2022) using a 5% poison rate on the VOC07 and VOC12 datasets. As shown in Table 3, CIB achieves approximately 15% higher ASR but significantly underperforms in Mean Average Precision (MAP), dropping by about 2% overall and around 20% for the source class. This reduction in MAP compromises its stealthiness. Additionally, our method extends to Image Regression and Semantic Segmentation tasks, where existing clean-image backdoors are ineffective. As illustrated in Table 3, our attack succeeds in these tasks, demonstrated



(a) CIFAR-10



(b) Tiny-ImageNet

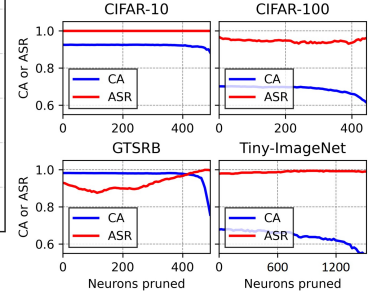


Figure 7: Fine-pruning.

by a substantial decrease in Attack Mean Square Error (AE) compared to the clean dataset. Detailed task configurations are provided in Appendix.

Ablation Study.

We conducted ablation studies on three key components of our design: GAN loss (for Existence), information loss (for Separability), and label condition (for Irrelevancy). The results are presented in Table 4.

(a) GAN Loss. We eliminate the discriminator D from C-InfoGAN and apply an l_∞ -norm constraint to the generator. Experiments show that this approach completely loses effectiveness because, without adversarial training, the trigger feature quickly overfits and becomes an adversarial attack on the recognition network Q , ceasing to function as an effective backdoor.

(b) Information Loss. Removing the information loss transforms our network into a standard Pix2Pix GAN. To perform the attack, we intuitively select the darkest 1% of images in the dataset as poisoned images to construct the trigger feature, modeling the trigger-wrapping problem as a style-transfer scenario solvable by Pix2Pix GAN. Under this setup, GCB significantly degrades in performance, indicating that manually designed triggers are ineffective.

(c) Label Condition. We remove y as a prior condition from all components in C-InfoGAN. The results show only a minor decrease in ASR, likely because the UNet generator preserves the original appearance, reducing the reliance on label conditioning. However, we observe that removing LC increases the likelihood of mode collapse, causing C-InfoGAN to generate uniform features. For a more detailed analysis of this effect, please refer to Appendix.

Stealthiness and Robustness Measure.

Stealthiness of GCB. We evaluated the stealthiness of our method using seven metrics from BackdoorBench (Wu et al. 2024). As shown in Fig. 6, clean-image backdoor attacks, such as FLIP and GCB, are significantly stealthier than poison-image backdoors like Blended (Chen et al. 2017) and IA (Nguyen and Tran 2020). Clean-image methods leverage benign features for the backdoor, creating poisoned data that closely resembles clean images. This makes them difficult to detect using image-quality metrics like SSIM and BRISQUE. While the Frechet Inception Distance (FID) assesses distributional differences, our experiments show that GCB excels

poison rate \rightarrow	1%	0.5%	0.1%
CIFAR-10			
(w/o L_{GAN})	8.97	4.14	1.90
(w/o L_{info})	42.9	11.4	2.87
(w/o LC)	98.9	93.1	85.3
Ours	100.0	100.0	98.5
CIFAR-100			
(w/o L_{GAN})	3.41	1.80	0.45
(w/o L_{info})	28.7	8.12	1.34
(w/o LC)	84.7	68.4	34.6
Ours	96.7	92.1	45.9

Table 4: Ablation Study.

Corruptions \downarrow	CA	ASR
Test-Time		
JPEG	77.6	100
Color Shift	84.4	98.4
Color Shrink	84.9	100
Affine	84.2	99.9
Training-Time		
JPEG	93.0	100
Color Shift	92.1	97.6
Color Shrink	92.3	99.8
Affine	91.8	100

Table 5: Robustness Under Different Corruptions.

here as well, with its triggered images closely matching the clean distribution across all tested metrics.

Robustness of GCB. To evaluate the robustness of GCB, we apply several common image corruption techniques, including JPEG Compression (Xue et al. 2023), Gaussian Smoothing (Xu, Evans, and Qi 2018), Color Shift (Jiang et al. 2023), Color Shrink (Xu, Evans, and Qi 2018), and Affine Transformation (Qiu et al. 2021). These transformations are widely recognized for their effectiveness in mitigating backdoor attacks. In our experiments, we apply these transformations at **test time** to each input image before feeding them into the victim model. The results in Table 5 demonstrate that GCB remains highly robust against these corruptions. While the CA drops by more than 10% in all cases, the ASR consistently remains close to 100%. Additional results on other baseline attacks and datasets are in Appendix.

Defenses

Classic Defenses

Neural Cleanse. Neural Cleanse (Wang et al. 2019) uses anomaly scores to detect backdoors in DNN models. However, Fig. 8 shows that Neural Cleanse is hard to differentiate backdoor-attacked datasets and clean ones, because their scores are similar and below the 2.0 threshold. This is due to Neural Cleanse’s focus on static adversarial patches, while our attack uses a dynamic, global trigger function, making trigger reconstruction difficult.

STRIP. STRIP (Gao et al. 2019) measures class prediction entropy through input perturbations. Fig. 9 shows a

Defense→	ABL		D-BR		CLP		EP		NAB		ASD		MSPC		ReBack		PIPD		Average
Attack↓	CA	ASR	CA	ASR	CA	ASR	CA	ASR	CA	ASR	CA	ASR	CA	ASR	CA	ASR	CA	ASR	ASR
BadNet	41.0	72.5	91.0	1.5	91.5	4.5	92.8	12.7	86.3	0.3	92.0	2.1	92.8	0.3	91.7	4.3	92.2	0.5	11.0
Blend	58.6	0.0	85.1	0.0	93.1	91.6	92.5	95.6	88.8	43.8	93.0	5.3	92.7	0.7	91.7	2.4	92.4	5.3	27.2
BPP	49.3	18.3	88.5	85.5	91.6	3.4	90.5	10.5	84.5	79.4	92.5	99.4	90.5	2.8	90.1	1.8	92.4	0.9	33.6
IA	62.5	31.5	85.3	84.8	84.7	10.3	90.1	6.7	90.2	74.4	92.3	19.8	92.5	5.3	87.9	1.7	91.3	4.0	26.5
SIG	54.3	50.1	91.3	49.6	93.1	79.0	92.1	83.6	90.1	82.1	92.2	99.5	91.0	10.3	87.4	29.9	92.5	13.6	55.3
SSBA	59.8	82.6	83.1	3.0	93.2	1.1	92.2	99.9	88.9	49.1	93.3	7.1	90.9	21.5	85.1	6.6	89.9	17.2	32.0
WaNet	77.3	26.2	84.3	60.2	90.5	0.8	89.9	63.3	89.9	11.7	91.7	8.8	93.0	54.2	90.2	84.4	92.7	11.4	35.7
FLIP	50.0	99.0	83.9	22.1	92.2	20.6	90.0	80.9	79.3	70.2	86.9	62.2	91.6	17.2	90.0	39.7	90.7	66.9	53.2
GCB	69.3	100.0	84.2	100.0	92.4	100.0	90.6	100.0	88.8	100.0	90.9	100.0	91.5	23.9	88.7	71.6	91.8	87.7	87.0

Table 6: Comparison of different attack methods against advanced backdoor defense methods.

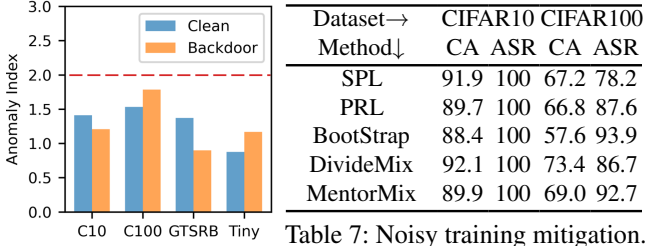


Figure 8: NC Defense.

Table 7: Noisy training mitigation. FLIP’s performance in Table 11.

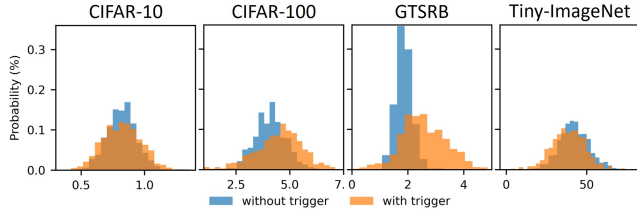


Figure 9: STRIP normalized entropy distribution of GCB.

notable similarity in entropy distribution for clean and poisoned subsets. Since C-InfoGAN uses benign features of various intensities as triggers, it can yield similar STRIP behaviors for samples with or without trigger. Therefore, our GCB attack is resilient to STRIP defense.

Fine-Pruning. Fine-Pruning (Liu, Dolan-Gavitt, and Garg 2018), which prunes high-activation neurons, is ineffective against our attack. Because our backdoor uses natural benign features, it creates a complex activation pattern that evades detection. Consequently, as shown in Fig. 7, the ASR on CIFAR-10 remains constant during pruning. On CIFAR-100, the ASR initially drops but then increases sharply, demonstrating the defense’s failure.

SOTA Backdoor Defenses

As shown in Table 6, we evaluated our attack against nine state-of-the-art (SOTA) backdoor defenses, including six since 2023 (Zheng et al. 2022; Liu, Sangiovanni-Vincentelli, and Yue 2023; Gao et al. 2023; Ma et al. 2024; Chen, Wu, and Zhou 2024; Pal et al. 2024). The proposed method, GCB, exhibits strong resistance against most of them. Only one defense, MSPC (Pal et al. 2024), proved effective, but most of the other attacks suffer from greater performance degradation. Even the latest defenses like ReBack (Ma et al. 2024) and PIPD (Chen, Wu, and Zhou 2024) failed to remove the

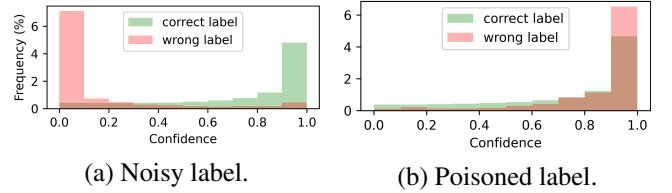


Figure 10: Confidence for two different label issues.

backdoor, only slightly lowering the ASR. We attribute this robustness to the attack’s inherent asymmetric trigger, where the training and testing triggers are different. This design bypasses the common assumption of latent separability (Qi et al. 2022) that many defenses rely on.

Adaptive Defenses

Noisy Training. Clean-image backdoors embed triggers by poisoning only labels. As a result, training techniques that are robust to label noise might diminish the effectiveness of these faulty labels. We evaluated five noisy training methods: Self-Paced Learning (SPL) (Kumar, Packer, and Koller 2010), Perturbation Robust Learning (PRL) (Wong and Kolter 2020), Bootstrap (Reed et al. 2014), DivideMix (Li, Socher, and Hoi 2020), and MentorMix (Jiang et al. 2020). As shown in Table 7, none of these methods effectively defend against our attack. This is likely because GCB’s incorrect labels constitute misleading knowledge rather than random noise, which contradicts the basic assumption of noisy training.

Label Cleaning. We evaluated the effectiveness of advanced label cleaning against GCB using CleanLab (Northcutt, Jiang, and Chuang 2021), a prominent tool for detecting label errors. Such methods work by flagging data with low model confidence. This successfully identifies random label noise, as the model cannot learn a coherent mapping, leading to low confidence scores (Fig. 10). In contrast, GCB intentionally creates a strong, learnable association between images and target labels. This results in poisoned samples having high confidence scores, rendering them indistinguishable from or even more confident than benign samples and making label cleaning an ineffective defense.

Conclusion

We introduced Generative Adversarial Clean-Image Backdoors (GCB), a stealthy and adaptive backdoor attack that

uses C-InfoGAN to optimize trigger patterns embedded within training images. Experiments across 6 datasets, 5 architectures, and 4 tasks showed high attack success rates with minimal drop in clean accuracy and low poison rates. GCB resists existing defenses, highlighting the need for more robust protections.

Ethical Implications

This work has clear dual-use implications. By showing that clean-image backdoors can achieve high attack success with negligible clean-accuracy degradation and very low poison rates, our method lowers the detection barrier for adversaries and could threaten safety-critical domains (e.g., medical imaging, autonomous driving) where model performance is tightly monitored. It also highlights a vulnerable point in the ML supply chain—data labeling—where malicious annotators can implant persistent failures without modifying pixels, and it demonstrates resilience against several existing defenses, potentially enabling longer dwell time for attacks. To mitigate misuse, we advocate (i) rigorous dataset provenance tracking and multi-party labeling/auditing; (ii) routine pre-deployment and continuous post-deployment backdoor screening, including behavior-level tests beyond patch reconstruction; (iii) training-time protections such as robust learning under suspected label noise and cross-source consistency checks; and (iv) defense-driven red-teaming before release. Any code artifacts should be accompanied by a usage license, clear risk disclosures, and guardrails (e.g., rate-limited models, withheld attack parameters) to reduce replication for abusive purposes. Ultimately, the primary ethical justification for releasing this research is to enable the community to build and evaluate stronger defenses against increasingly stealthy data-centric attacks.

References

- Amula, V. A.; Samavedam, S.; Saini, S.; Gupta, A.; and Narayanan, P. 2025. Prototype Guided Backdoor Defense via Activation Space Manipulation. In *Proceedings of the IEEE/CVF International Conference on Computer Vision*, 2195–2205.
- An, S.; Yao, Y.; Xu, Q.; Ma, S.; Tao, G.; Cheng, S.; Zhang, K.; Liu, Y.; Shen, G.; Kelk, I.; et al. 2023. ImU: Physical Impersonating Attack for Face Recognition System with Natural Style Changes. In *2023 IEEE Symposium on Security and Privacy (SP)*, 899–916. IEEE Computer Society.
- Chen, K.; Lou, X.; Xu, G.; Li, J.; and Zhang, T. 2022. Clean-image backdoor: Attacking multi-label models with poisoned labels only. In *The Eleventh International Conference on Learning Representations*.
- Chen, X.; Duan, Y.; Houthooft, R.; Schulman, J.; Sutskever, I.; and Abbeel, P. 2016. Infogan: Interpretable representation learning by information maximizing generative adversarial nets. *Advances in neural information processing systems*, 29.
- Chen, X.; Liu, C.; Li, B.; Lu, K.; and Song, D. 2017. Targeted backdoor attacks on deep learning systems using data poisoning. *arXiv preprint arXiv:1712.05526*.
- Chen, Y.; Wu, H.; and Zhou, J. 2024. Progressive poisoned data isolation for training-time backdoor defense. In *Proceedings of the AAAI Conference on Artificial Intelligence*, volume 38, 11425–11433.
- Deng, J.; Dong, W.; Socher, R.; Li, L.-J.; Li, K.; and Fei-Fei, L. 2009. Imagenet: A large-scale hierarchical image database. In *2009 IEEE conference on computer vision and pattern recognition*, 248–255. Ieee.
- Dosovitskiy, A.; Beyer, L.; Kolesnikov, A.; Weissenborn, D.; Zhai, X.; Unterthiner, T.; Dehghani, M.; Minderer, M.; Heigold, G.; Gelly, S.; et al. 2020. An Image is Worth 16x16 Words: Transformers for Image Recognition at Scale. In *International Conference on Learning Representations*.
- Everingham, M.; Eslami, S. A.; Van Gool, L.; Williams, C. K.; Winn, J.; and Zisserman, A. 2015. The pascal visual object classes challenge: A retrospective. *International journal of computer vision*, 111: 98–136.
- Gao, K.; Bai, Y.; Gu, J.; Yang, Y.; and Xia, S.-T. 2023. Backdoor defense via adaptively splitting poisoned dataset. In *Proceedings of the IEEE/CVF Conference on Computer Vision and Pattern Recognition*, 4005–4014.
- Gao, Y.; Xu, C.; Wang, D.; Chen, S.; Ranasinghe, D. C.; and Nepal, S. 2019. STRIP: A Defence Against Trojan Attacks on Deep Neural Networks. In *35th Annual Computer Security Applications Conference (ACSAC)*.
- Goodfellow, I.; Pouget-Abadie, J.; Mirza, M.; Xu, B.; Warde-Farley, D.; Ozair, S.; Courville, A.; and Bengio, Y. 2014. Generative adversarial nets. *Advances in neural information processing systems*, 27.
- Gu, T.; Liu, K.; Dolan-Gavitt, B.; and Garg, S. 2019. Badnets: Evaluating backdooring attacks on deep neural networks. *IEEE Access*, 7: 47230–47244.
- Han, X.; Xu, G.; Zhou, Y.; Yang, X.; Li, J.; and Zhang, T. 2022. Physical backdoor attacks to lane detection systems in autonomous driving. In *Proceedings of the 30th ACM International Conference on Multimedia*, 2957–2968.
- He, K.; Zhang, X.; Ren, S.; and Sun, J. 2016. Identity mappings in deep residual networks. In *Computer Vision—ECCV 2016: 14th European Conference, Amsterdam, The Netherlands, October 11–14, 2016, Proceedings, Part IV 14*, 630–645. Springer.
- Jang, E.; Gu, S.; and Poole, B. 2016. Categorical Reparameterization with Gumbel-Softmax. In *International Conference on Learning Representations*.
- Jha, R.; Hayase, J.; and Oh, S. 2024. Label poisoning is all you need. *Advances in Neural Information Processing Systems*, 36.
- Jiang, L.; Huang, D.; Liu, M.; and Yang, W. 2020. Beyond synthetic noise: Deep learning on controlled noisy labels. In *International conference on machine learning*, 4804–4815. PMLR.
- Jiang, W.; Li, H.; Xu, G.; and Zhang, T. 2023. Color Backdoor: A Robust Poisoning Attack in Color Space. In *Proceedings of the IEEE/CVF Conference on Computer Vision and Pattern Recognition*, 8133–8142.

- Karras, T.; Laine, S.; and Aila, T. 2019. A style-based generator architecture for generative adversarial networks. In *Proceedings of the IEEE/CVF conference on computer vision and pattern recognition*, 4401–4410.
- Krizhevsky, A. 2009. Learning Multiple Layers of Features from Tiny Images. *Master's thesis, University of Tront*.
- Kumar, M.; Packer, B.; and Koller, D. 2010. Self-paced learning for latent variable models. *Advances in neural information processing systems*, 23.
- LeCun, Y.; Bottou, L.; Bengio, Y.; and Haffner, P. 1998. Gradient-based learning applied to document recognition. *Proceedings of the IEEE*, 86(11): 2278–2324.
- Li, J.; Socher, R.; and Hoi, S. C. 2020. DivideMix: Learning with Noisy Labels as Semi-supervised Learning. In *International Conference on Learning Representations*.
- Li, Y.; Jiang, Y.; Li, Z.; and Xia, S.-T. 2022. Backdoor learning: A survey. *IEEE Transactions on Neural Networks and Learning Systems*.
- Li, Y.; Zhai, T.; Wu, B.; Jiang, Y.; Li, Z.; and Xia, S. 2020. Rethinking the trigger of backdoor attack. *arXiv preprint arXiv:2004.04692*.
- Li, Y.; Zhao, J.; Lv, Z.; and Li, J. 2021. Medical image fusion method by deep learning. *International Journal of Cognitive Computing in Engineering*, 2: 21–29.
- Liu, K.; Dolan-Gavitt, B.; and Garg, S. 2018. Fine-pruning: Defending against backdooring attacks on deep neural networks. In *International symposium on research in attacks, intrusions, and defenses*, 273–294. Springer.
- Liu, M.; Sangiovanni-Vincentelli, A.; and Yue, X. 2023. Beating Backdoor Attack at Its Own Game. In *Proceedings of the IEEE/CVF International Conference on Computer Vision*, 4620–4629.
- Liu, Y.; Ma, X.; Bailey, J.; and Lu, F. 2020. Reflection backdoor: A natural backdoor attack on deep neural networks. In *Computer Vision—ECCV 2020: 16th European Conference, Glasgow, UK, August 23–28, 2020, Proceedings, Part X 16*, 182–199. Springer.
- Liu, Z.; Luo, P.; Wang, X.; and Tang, X. 2015. Deep Learning Face Attributes in the Wild. In *Proceedings of International Conference on Computer Vision (ICCV)*.
- Ma, Z.; Yang, Y.; Liu, Y.; Yang, T.; Liu, X.; Li, T.; and Qin, Z. 2024. Need for Speed: Taming Backdoor Attacks with Speed and Precision. In *2024 IEEE Symposium on Security and Privacy (SP)*, 1217–1235. IEEE.
- Mirza, M.; and Osindero, S. 2014. Conditional generative adversarial nets. *arXiv preprint arXiv:1411.1784*.
- Nguyen, T. A.; and Tran, A. 2020. Input-aware dynamic backdoor attack. *Advances in Neural Information Processing Systems*, 33: 3454–3464.
- Northcutt, C. G.; Jiang, L.; and Chuang, I. L. 2021. Confident Learning: Estimating Uncertainty in Dataset Labels. *Journal of Artificial Intelligence Research (JAIR)*, 70: 1373–1411.
- Pal, S.; Yao, Y.; Wang, R.; Shen, B.; and Liu, S. 2024. Backdoor Secrets Unveiled: Identifying Backdoor Data with Optimized Scaled Prediction Consistency. In *The Twelfth International Conference on Learning Representations*.
- Qi, X.; Xie, T.; Li, Y.; Mahloujifar, S.; and Mittal, P. 2022. Revisiting the assumption of latent separability for backdoor defenses. In *International Conference on Learning Representations*.
- Qiu, H.; Zeng, Y.; Guo, S.; Zhang, T.; Qiu, M.; and Thuraisingham, B. 2021. Deepsweep: An evaluation framework for mitigating DNN backdoor attacks using data augmentation. In *Proceedings of the 2021 ACM Asia Conference on Computer and Communications Security*, 363–377.
- Reed, S.; Lee, H.; Anguelov, D.; Szegedy, C.; Erhan, D.; and Rabinovich, A. 2014. Training deep neural networks on noisy labels with bootstrapping. *arXiv preprint arXiv:1412.6596*.
- Rong, D.; Shen, S.; Fu, X.; Qian, P.; Chen, J.; He, Q.; Fu, X.; and Wang, W. 2024. Clean-image Backdoor Attacks. *arXiv preprint arXiv:2403.15010*.
- Russakovsky, O.; Deng, J.; Su, H.; Krause, J.; Satheesh, S.; Ma, S.; Huang, Z.; Karpathy, A.; Khosla, A.; Bernstein, M.; et al. 2015. Imagenet large scale visual recognition challenge. *International journal of computer vision*, 115: 211–252.
- Simonyan, K.; and Zisserman, A. 2015. Very deep convolutional networks for large-scale image recognition. In *3rd International Conference on Learning Representations (ICLR 2015)*. Computational and Biological Learning Society.
- Stallkamp, J.; Schlipsing, M.; Salmen, J.; and Igel, C. 2012. Man vs. computer: Benchmarking machine learning algorithms for traffic sign recognition. *Neural networks*, 32: 323–332.
- Tan, M.; and Le, Q. 2019. Efficientnet: Rethinking model scaling for convolutional neural networks. In *International conference on machine learning*, 6105–6114. PMLR.
- Turner, A.; Tsipras, D.; and Madry, A. 2019. Label-consistent backdoor attacks. *arXiv preprint arXiv:1912.02771*.
- Vaswani, A.; Shazeer, N.; Parmar, N.; Uszkoreit, J.; Jones, L.; Gomez, A. N.; Kaiser, Ł.; and Polosukhin, I. 2017. Attention is all you need. *Advances in neural information processing systems*, 30.
- Wang, B.; Yao, Y.; Shan, S.; Li, H.; Viswanath, B.; Zheng, H.; and Zhao, B. Y. 2019. Neural cleanse: Identifying and mitigating backdoor attacks in neural networks. In *2019 IEEE Symposium on Security and Privacy (SP)*. IEEE.
- Wei, S.; Zhang, M.; Zha, H.; and Wu, B. 2024. Shared adversarial unlearning: Backdoor mitigation by unlearning shared adversarial examples. *Advances in Neural Information Processing Systems*, 36.
- Wong, E.; and Kolter, J. Z. 2020. Learning perturbation sets for robust machine learning. *arXiv preprint arXiv:2007.08450*.
- Wu, B.; Chen, H.; Zhang, M.; Zhu, Z.; Wei, S.; Yuan, D.; Zhu, M.; Wang, R.; Liu, L.; and Shen, C. 2024. BackdoorBench: A Comprehensive Benchmark and Analysis of Backdoor Learning. *arXiv:2407.19845*.
- Xia, W.; Zhang, Y.; Yang, Y.; Xue, J.-H.; Zhou, B.; and Yang, M.-H. 2022. Gan inversion: A survey. *IEEE Transactions on Pattern Analysis and Machine Intelligence*, 45(3).
- Xu, W.; Evans, D.; and Qi, Y. 2018. Feature Squeezing: Detecting Adversarial Examples in Deep Neural Networks. In

Proceedings 2018 Network and Distributed System Security Symposium. Internet Society.

Xue, M.; Wang, X.; Sun, S.; Zhang, Y.; Wang, J.; and Liu, W. 2023. Compression-resistant backdoor attack against deep neural networks. *Applied Intelligence*, 1–16.

Zeng, Y.; Pan, M.; Just, H. A.; Lyu, L.; Qiu, M.; and Jia, R. 2023. Narcissus: A practical clean-label backdoor attack with limited information. In *Proceedings of the 2023 ACM SIGSAC Conference on Computer and Communications Security*, 771–785.

Zhao, P.; Chen, P.-Y.; Das, P.; Ramamurthy, K. N.; and Lin, X. 2020. Bridging Mode Connectivity in Loss Landscapes and Adversarial Robustness. In *International Conference on Learning Representations*.

Zheng, R.; Tang, R.; Li, J.; and Liu, L. 2022. Pre-activation distributions expose backdoor neurons. *Advances in Neural Information Processing Systems*, 35: 18667–18680.

Zhu, M.; Wei, S.; Shen, L.; Fan, Y.; and Wu, B. 2023. Enhancing fine-tuning based backdoor defense with sharpness-aware minimization. In *Proceedings of the IEEE/CVF International Conference on Computer Vision*, 4466–4477.

Zhu, M.; Wei, S.; Zha, H.; and Wu, B. 2024. Neural polarizer: A lightweight and effective backdoor defense via purifying poisoned features. *Advances in Neural Information Processing Systems*, 36.

Breaking the Stealth-Potency Trade-off in Clean-Image Backdoors with Generative Trigger Optimization

Supplementary Material

Mathematical Analysis

In this section, we analyze why optimizing C-InfoGAN leads to the optimization of our clean-image backdoor task. C-InfoGAN, a variant of InfoGAN (Chen et al. 2016), is adapted to select a subset of images for poisoning and design a trigger function. Given InfoGAN’s well-established convergence properties (Goodfellow et al. 2014), we focus on the alignment between C-InfoGAN’s objectives and the backdoor attack, emphasizing the role of the scoring function $s(x)$.

C-InfoGAN Analysis

C-InfoGAN extends InfoGAN by conditioning the generator G and mutual information estimator Q on the input image x and a binary code $c \in \{0, 1\}$, where $p(c = 1) = p_r$ (the poison rate) and $p(c = 0) = 1 - p_r$. The loss comprises the standard GAN objective and a mutual information term:

$$L = \min_G \max_D \mathbb{E}_{x \sim p(x)} [\log D(x)] + \mathbb{E}_{\hat{x} \sim p(\hat{x})} [\log(1 - D(\hat{x}))] - \lambda I(c; G(x, c)), \quad (1)$$

where $\hat{x} = G(x, c)$, and $I(c; G(x, c))$ is maximized via a variational lower bound using Q :

$$L_I(G, Q) = \mathbb{E}_{\hat{x} \sim G(x, c)} [\mathbb{E}_{c' \sim p(c|\hat{x})} [\log Q(c'|\hat{x})]] + H(c). \quad (2)$$

When trained sufficiently, C-InfoGAN exhibits the following properties:

- $p(\hat{x}) \approx p(x)$, as the generator aligns the generated distribution with the real data distribution.
- $Q(c|\hat{x}) \approx p(c|\hat{x})$, enabling accurate estimation of the code c from \hat{x} .
- $I(c; G(x, c))$ is maximized, making $p(\hat{x}_0)$ and $p(\hat{x}_1)$ —where $\hat{x}_0 = G(x, c = 0)$ and $\hat{x}_1 = G(x, c = 1)$ —as distinct as possible, with weights $1 - p_r$ and p_r , respectively.

Define the scoring function $s(x) = Q(c = 1|x) - Q(c = 0|x)$. Data is partitioned into $X_0 = \{x \in X \mid s(x) < 0\}$ and $X_1 = \{x \in X \mid s(x) \geq 0\}$, with corresponding distributions $p(x_0)$ and $p(x_1)$. Since Q approximates $p(c|\hat{x})$ optimally, $s(x)$ effectively distinguishes \hat{x}_0 and \hat{x}_1 , and, given $p(\hat{x}_0) \approx p(x_0)$ and $p(\hat{x}_1) \approx p(x_1)$, it aligns the real and generated partitions. Since C-InfoGAN is a special case of InfoGAN, we refer readers to Chen et al. (2016) for detailed proofs and focus here on its application to our task.

Scoring Function Analysis

The scoring function $s(x)$ is pivotal to our backdoor attack. It selects X_1 , the poisoned subset, as the top p_r fraction of images ranked by $s(x)$. To understand its effectiveness, consider the mutual information objective:

$$I(c; G(x, c)) = (1 - p_r) \text{KL}(p(\hat{x}_0) \parallel p(\hat{x})) + p_r \text{KL}(p(\hat{x}_1) \parallel p(\hat{x})), \quad (3)$$

where $p(\hat{x}) = (1 - p_r)p(\hat{x}_0) + p_r p(\hat{x}_1)$. This is equivalent to the weighted Jensen-Shannon divergence:

$$I(c; G(x, c)) = \text{JSD}_{1-p_r, p_r}(p(\hat{x}_0) \parallel p(\hat{x}_1)).$$

Maximizing $I(c; G(x, c))$ thus maximizes the distinction between $p(\hat{x}_0)$ and $p(\hat{x}_1)$. Since $p(\hat{x}_0) \approx p(x_0)$ and $p(\hat{x}_1) \approx p(x_1)$ upon convergence, $s(x)$ induces a partition where $p(x_0)$ and $p(x_1)$ are similarly distinct. Conditionally, training G , D , and Q on the ground-truth label y yields:

$$\max \text{JSD}(p(x_1|y) \parallel p(x_0|y)),$$

ensuring X_1 is distinguishable from X_0 within each class.

Connection to Clean-Image Backdoors

In our clean-image backdoor attack, X_1 images have labels flipped to a target class y_t , and the trigger $T(x) = G(x, c = 1)$ transforms benign images to mimic X_1 . The victim model f^* is:

$$f^*(x) = \arg \min_f \left[\sum_{(x_0, y_0) \in (X_0, Y_0)} L(f(x_0), y_0) + \sum_{x_1 \in X_1} L(f(x_1), y_t) \right], \quad (4)$$

with the attack success rate (ASR) defined as:

$$\text{ASR} = \mathbb{E}_{x \sim p(x)} \mathbb{1}[f^*(T(x)) = y_t].$$

We optimize this in two steps:

Optimizing X_1 : The model must associate X_1 with y_t while preserving accuracy on X_0 . This requires minimizing the conditional entropy $H(Y'|X)$, where Y' is the poisoned label distribution ($y' = y_t$ if $x \in X_1$, else $y' = y$). Expanding:

$$H(Y'|X) = H(Y') + H(X|Y') - H(X).$$

Since $H(X)$ is constant and $H(Y')$ is minimized by the poisoning strategy, the problem reduces to:

$$\min H(X|Y') = H(X|C, Y),$$

where $c = 1$ if $x \in X_1$, else $c = 0$, and $H(Y'|C, Y) = 0$. For c independent of y :

$$H(X|C, Y) = H(X|Y) - \text{JSD}_{p_r, 1-p_r}(p(x_1|y) \parallel p(x_0|y)),$$

with $H(X|Y)$ constant. Thus, maximizing $\text{JSD}(p(x_1|y) \parallel p(x_0|y))$ —achieved via C-InfoGAN—minimizes $H(Y'|X)$, enhancing the backdoor’s learnability.

Optimizing T : The trigger must satisfy:

$$\min \text{JSD}(p(T(x)|y) \parallel p(x_1|y)).$$

Since $T(x) = G(x, c = 1) = \hat{x}_1$, and C-InfoGAN minimizes $\text{JSD}(p(\hat{x}_1|y) \parallel p(x_1|y))$, $T(x)$ effectively mimics X_1 , triggering the backdoor.

Discussion on Assumptions

Our analysis assumes C-InfoGAN converges such that $p(\hat{x}) \approx p(x)$ and $Q(c|\hat{x}) \approx p(c|x)$. While GAN convergence can be imperfect in practice, we employ stabilization techniques (e.g., gradient penalties) to ensure robustness. Empirical results validate that approximate convergence suffices for high ASR, bridging theory and practice.

Understanding GCB’s Asymmetry

Our experimental results demonstrate that GCB achieves excellent attack performance, evidenced by high Clean Accuracy (CA) and Attack Success Rates (ASR) (see Figures 3, 4, and 5). Additionally, GCB exhibits robustness and resilience against defenses, as shown in Tables 5, 6, 7 and Figures 8, 9, and 7.

Achieving both high ASR and robustness is particularly intriguing because, typically, attacks that converge quickly and attain high ASR are more easily detected by simple defense methods. The primary reason for GCB’s effectiveness in both metrics is that it is inherently an *asymmetric backdoor* attack. During the poisoning stage, the images of poisoned samples contain relatively weak trigger information, which makes training-stage defenses less effective. In contrast, during the inference stage, the generated triggered images carry very strong trigger information, resulting in a high ASR.

We provide a visualization of this phenomenon in Figure 11, which illustrates how we select samples to poison and add triggers in the two stages from the perspective of the latent space.

In the poisoning stage, we use a score function to evaluate all samples and select those with the highest scores for poisoning. These selected images carry varying degrees of trigger information (depending on their scores), resulting in a gradual change in trigger information. This gradual change makes the poisoned samples undetachable from benign samples, making them harder to detect (Qi et al. 2022). This characteristic ensures robustness against common defenses.

During the inference stage, we apply a trigger function to generate triggers. The generated triggers follow a slightly different distribution from the selected samples in the poisoning stage. They are significantly distant from benign samples in the latent space, which increases the likelihood of activating the backdoor and causing misclassification to the target label. This inherent asymmetric design of triggers in our GCB attack enables it to maintain both high ASR and robustness simultaneously.

Experimental Settings

C-InfoGAN Settings

In our model, the ground-truth label y is combined with the poison condition c , and integrated into the image feature map through cross-attention mechanisms (Vaswani et al. 2017) at each convolutional layer in the UNet structure. For all experiments, we apply batch normalization after most layers and set the random seed to 42 to ensure reproducible results. The temperature of the Gumbel Softmax (Jang, Gu, and Poole 2016) is set at 0.5. The batch size for all experiments is 256, with a weight decay of $1e-5$. We use the Adam optimizer with

betas of 0.5 and 0.999 for training for 100 epochs on each dataset. Both the generator and discriminator steps are set to 1. Following InfoGAN (Chen et al. 2016), we identified that certain parameters, such as the learning rate and information loss weight, are crucial for convergence. The hyperparameters for the learning rate and information loss weight for different structures are presented in Table 8. It is important to note that the provided hyperparameters are not the only set that can achieve convergence, but they demonstrate how to produce the results in this paper. All models are trained on Nvidia A100 for no more than 2 hours to get converged.

Dataset	lr G	lr D	λ
MNIST	5e-4	1e-4	0.5
CIFAR-10	4e-5	4e-5	0.25
CIFAR-100	4e-4	2e-4	0.25
GTSRB	4e-5	4e-5	0.25
ColorCIFAR10	4e-5	4e-5	0.25
CelebA	4e-4	4e-4	0.1
VOC2012	4e-4	4e-4	0.1

Table 8: Important hyperparameters setting in our experiment.

Victim Model Setting

Unless specified, we use PreActResNet18 as the default victim model, and 0.01 as the default poison rate. For the training victim model, SGD with momentum of 0.9 is used under batch size of 128 and weight decay of 0.0005. A cosine learning rate scheduler with an initial learning rate of 0.01 is also used for stable convergence. For CIFAR-10 and CIFAR-100, we use 100 epoch as the default setting. For simpler datasets like MNIST or GTSRB, we use 20 and 50 as default epochs for quicker testing. All experiments on GCB are carried out in an all-to-one fashion.

Other Vision Task Setting

CIB (Chen et al. 2022) Details. We carried out our multi-label experiment based on the official code of CIB (Chen et al. 2022). We find that CIB can be highly sensitive to various source classes. To provide a more statistically significant result, we systematically tested each possible source class within the training dataset, calculating both the mean and standard deviation. For CIB one-to-one setting, we considered all label combinations with proportion of $5\pm 1\%$ as potential source classes.

Dataset. *Image Regression:* We introduce ColorCIFAR-10, derived from CIFAR-10 (Krizhevsky 2009), with labels representing continuous features: hue, saturation, and illumination. Cyclic encoding is used for hue, resulting in four labels (sin hue, cos hue, saturation, illumination), each scaled to $[-1, 1]$ with added Gaussian noise ($\mathcal{N}(0, 0.1^2)$) and clipped to $[-1, 1]$. *Semantic Segmentation:* VOC2012 (Everingham et al. 2015) is used with a focus on samples with semantic segmentation annotations, totaling 2,330 training and 583 testing images. *Multi-label Binary Classification:* CelebA (Liu et al. 2015) is utilized with five balanced and independent binary labels: Attractive, Mouth Slightly Open, High Cheekbones, Smiling, Wavy Hair.

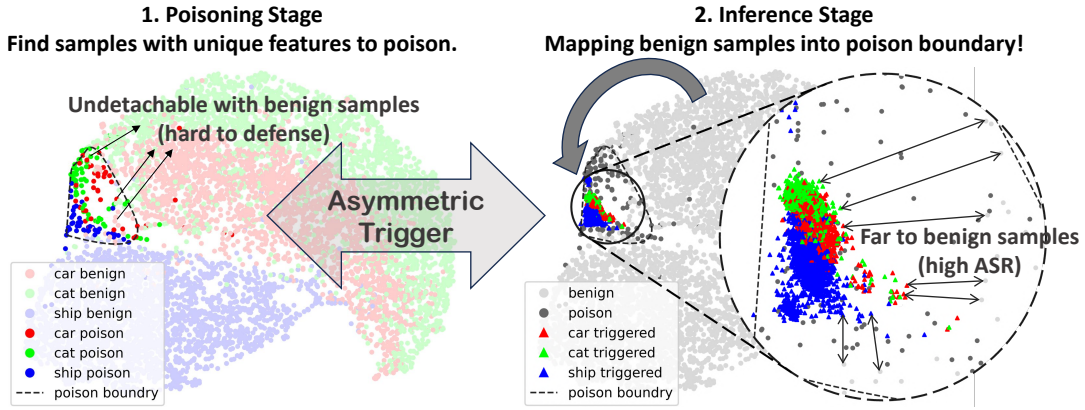


Figure 11: UMAP visualization of the latent space for three classes in CIFAR-10. **Left:** Poisoning Stage—We select samples with unique features to poison; these samples are undetachable from clean samples, making them hard to detect. **Right:** Inference Stage—We use a trigger function to map benign images into the poisoned boundary to trigger the backdoor. Triggered images are mapped to a small area within the poisoned boundary, making them far from benign images and resulting in a high ASR.

Architecture. In training InfoGAN, cross-attention is employed for class feature encoding in all tasks. For Image Regression and Multi-label Binary Classification, labels are directly fed to cross-attention without preprocessing. For Semantic Segmentation, label images are added to the UNet image channels, bypassing cross-attention. Victim models are trained using PreActResNet18 for Image Regression and Multi-label Binary Classification, and UNet for Semantic Segmentation. All models undergo 100 epochs of training with SGD, an initial learning rate of 0.01, weight decay of 0.0005, and a standard cosine scheduler.

Architecture	FLIP		GCB	
	CA	ASR	CA	ASR
EfficientNet-B0	74.9%	3.8%	73.0%	99.93%
PreActResNet18	91.9%	86.3%	92.6%	100.0%
ResNet18	83.4%	4.9%	84.3%	100.0%
VGG19	88.6%	5.6%	89.5%	100.0%
ViT-B-16	95.2%	3.4%	94.5%	100.0%

Table 9: Comparison of FLIP and our attack across architectures. FLIP, trained on a PreActResNet18 surrogate model, performs well only when the victim model matches the surrogate. In contrast, our attack is effective across all architectures.

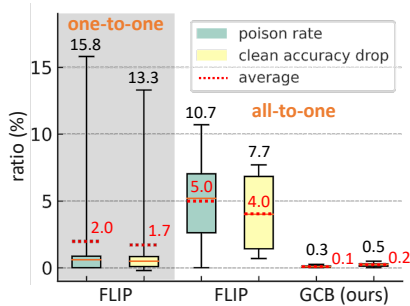


Figure 12: Box plot comparing the class-wise clean accuracy (CA) drop for clean-image backdoors on CIFAR-10. While the SOTA method, FLIP, has a low average CA drop (1.7%), it can reach as high as 13.3% for the source class. In contrast, our method exhibits a negligible CA drop across all classes.

Discussion on FLIP (Jha, Hayase, and Oh 2024)

FLIP Experiment Setup. We carry out our experiment based on the official code of FLIP and BackdoorBench (Wu et al. 2024). In FLIP, the source class is set to all classes and the target class to class 0, aiming for an all-to-one attack. Poisoned labels for all samples are generated using FLIP and then sent to BackdoorBench for a fair comparison.

Weakness of FLIP. There are two major weakness of FLIP. The first one is that it is extremely sensitive to different architectures of victim models, as shown in Table 9. FLIP and our proposed method, GCB, were tested on different victim model architectures using the CIFAR-10 dataset. FLIP uses 3% poison rate, and GCB uses 1% poison rate. Since FLIP’s expert model defaults to PreActResNet34, it performs well on similar architectures like PreActResNet18. However, FLIP fails to poison all other architectures, making it impractical in real scenarios because adversaries are unlikely to anticipate the victim model’s structure.

The second major weakness is that FLIP suffers from high CA drop in both one-to-one ¹ scenario and all-to-one ² scenario. For the one-to-one scenario, although the mean CA drop seems low, it is an averaged result across all classes. When considering the CA drop of the source class, it will surprisingly become 13.3%. For the all-to-one scenario, the CA drop is consistently as large as 4%.

¹one source class and one target class

²all except the target class are regarded as the source class

ASR vs Poison Rates

We provide the ASR versus poison rate as an additional result, particularly for positioning the CIBA attack on CIFAR-10. Since they do not release their code, we can only replicate their results here rather than directly compare them in the same benchmark as other attack methods in Fig. 3.

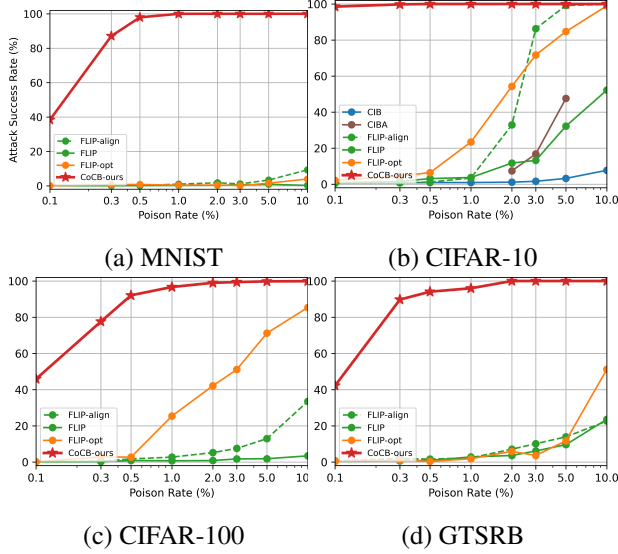


Figure 13: ASR vs. poison rates for different attack methods.

GCB’s Robustness to Dataset Size

We evaluate the robustness of GCB under varying training dataset sizes on CIFAR-10 and CIFAR-100. As shown in Figure 14, GCB maintains high attack success rates (ASR) even when the dataset size is reduced, demonstrating its stability and efficiency with limited data. While performance slightly decreases in extremely small datasets, this degradation is consistent with a significant drop in clean accuracy (CA), indicating that GCB’s effectiveness is not disproportionately affected by dataset size.

GCB’s Robustness to Architectures

We evaluated our attack’s robustness across various target model structures, including PreActResNet18(He et al. 2016), EfficientNet B0(Tan and Le 2019), VGG11(Simonyan and Zisserman 2015), and ViT-B-16(Dosovitskiy et al. 2020), chosen for their unique efficiencies, accuracies, and scalability. As Table 10 shows, our attack consistently achieves high ASR across these different architectures, implying model-agnostic traits. PreActResNet18, maintaining good CA while reaching the lowest ASR, is chosen as the basic architecture for all other experiments.

Poisoned Sample Visualization

Poison Samples in Image Classification

As shown in Fig. 15, in our experiments, C-InfoGAN predominantly identified color as the trigger feature for all datasets

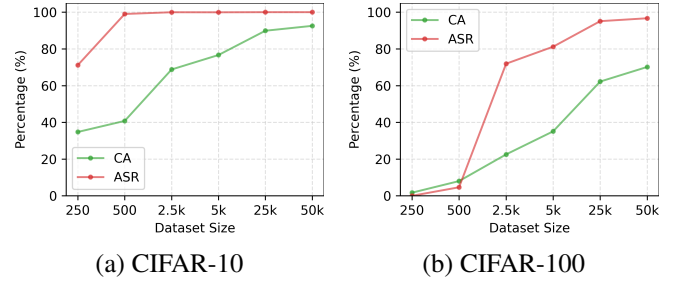


Figure 14: Results under different dataset sizes for CIFAR-10/100. Both CIFAR-10/100 have 50,000 images in total. Results show that GCB remains effective in most cases. When GCB lose effectiveness, the clean accuracy of each method also significantly drops to less than 10%.

Architecture	PreActRN18		VGG11		EffNet B0		ViT-B-16	
Dataset	CA	ASR	CA	ASR	CA	ASR	CA	ASR
MNIST	98.5	100	98.4	100	98.6	100	98.6	100
CIFAR10	92.6	100	88.3	100	73.0	99.9	94.5	100
CIFAR100	70.1	96.7	58.6	93.0	52.9	93.8	84.1	95.3
GTSRB	95.9	96.0	93.7	96.2	85.0	91.2	98.0	95.2
Average	89.3	98.2	84.8	97.3	77.4	96.2	93.8	97.6

Table 10: CA and ASR of different architectures of poison rate 1%. Our model shows high ASR across all tested datasets and models.

except MNIST for its irrelevance to class information. Occasionally, this color trigger was combined with positional or global contrast features. For the MNIST dataset, where images are grayscale and normalized, the model adapted by learning more semantic features, such as the weight or thickness of digits, as triggers. Thus, C-InfoGAN is effective in identifying dominant semantic features unrelated to class labels as triggers.

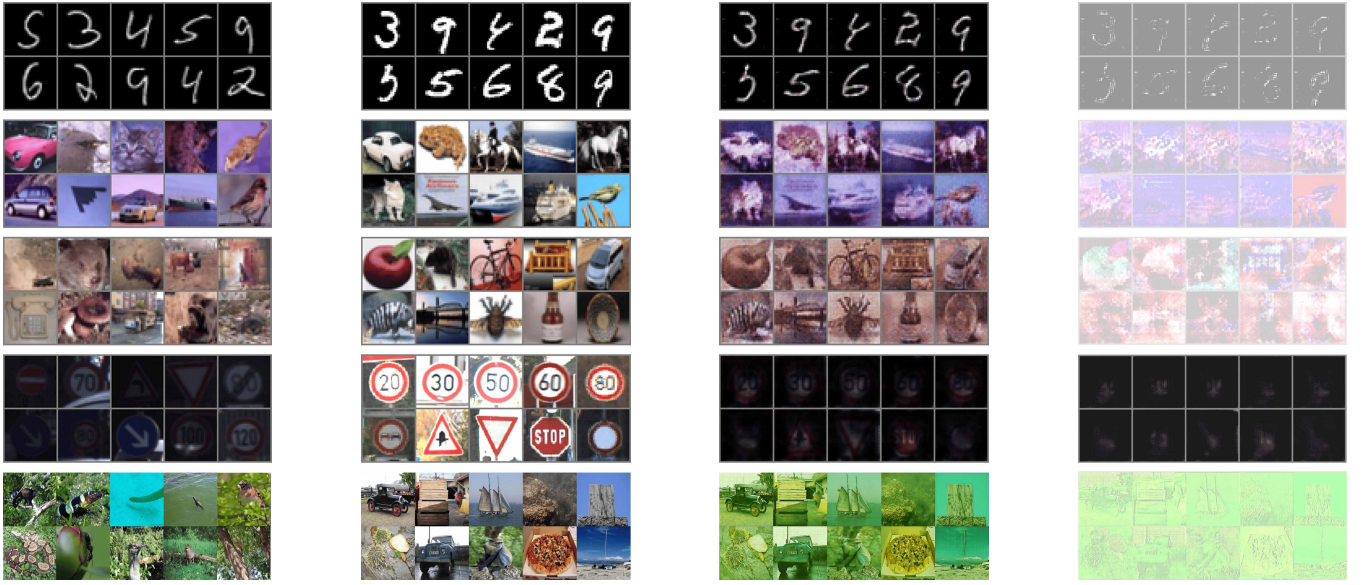
Poison Samples in Other Tasks

Analyzing the triggered features generated for each dataset reveals interesting distinctions. As shown in Fig. 16, VOC2012 retains color features similar to image classification tasks. In contrast, CelebA, where color might be label-relevant, learns background color as the triggered feature. Most notably, ColorCIFAR-10 selects image borders as the trigger, attributed to the prevalence of bordered images in the dataset. This suggests that InfoGAN can be directed to specific features by incorporating relevant priors, thereby avoiding unwanted feature learning.

Robustness Measure

Although clean-image backdoors do not poison images during training, triggers are still used to activate the backdoor at test time. To evaluate test-time preprocessing defenses, we assess several prominent techniques in our experiments:

1. **JPEG Compression** (Xue et al. 2023): Applies JPEG compression to all testing images at 75% quality.



(a) Selected train images (b) Clean test images (c) Triggered test images (d) Trigger in differences

Figure 15: Sample images from MNIST, CIFAR-10, CIFAR-100, GTSRB, and ImageNet-1K. The selected training images are unmodified, representing a subset of clean images.

2. **Gaussian Smoothing** (Xue et al. 2023): Applies Gaussian blur with a kernel size of 3 pixels to each image.
3. **Color Shift** (Jiang et al. 2023): Introduces a random color space shift between -0.1 and 0.1, specifically targeting color-based backdoors in datasets like CIFAR-10.
4. **Color Shrink** (Li et al. 2020): Reduces the color-bit depth of test images to 5 bits.
5. **Affine Transformation** (Qiu et al. 2021): Applies stochastic affine transformation to each test image as a defense.

Table 12 presents the results of these preprocessing defenses on the CIFAR-10 and CIFAR-100 datasets. Additive trigger-based attacks, such as BadNets, exhibit reduced ASR when subjected to image transformations. Natural trigger-based attacks like SIG and FLIP remain robust against most defenses but are compromised by image compression. In contrast, our GCB attack maintains nearly 100% ASR across all preprocessing defenses on CIFAR-10 and is also effective on CIFAR-100. This resilience is attributed to the use of a dominant semantic feature as the trigger, which is more robust than fragile and intricate label features.

GCB's Resilience

GCB's Resilience on Clean-Data-Based Defenses

In Table 6 in our paper, we already show poison-data-based backdoor defenses. There is also one branch of backdoor defense called clean-data-based backdoor defenses, where they assume the defender to have additional private in-distribution clean data (typically 5% 10% of the whole dataset). To evaluate these methods, we show the results in Table 13. As shown, our GCB is defended by FT-SAM and SAU, which are very recent defenses in 2023 and 2024, respectively. As a result, the conclusion here is: although not designed to be, our method

Dataset→	CIFAR10				CIFAR100			
Attack→	GCB (ours)		FLIP-opt		GCB (ours)		FLIP-opt	
Method↓	CA	ASR	CA	ASR	CA	ASR	CA	ASR
No Defense	92.6	100	90.5	78.2	70.2	96.7	67.1	64.9
SPL	91.9	100	84.5	9.4	67.2	78.2	56.1	48.8
PRL	89.7	100	88.5	82.8	66.8	87.6	66.2	47.9
BootStrap	88.4	100	92.2	14.3	57.6	93.9	59.9	94.4
DivideMix	92.1	100	89.1	24.4	73.4	86.7	65.4	64.5
MentorMix	89.9	100	89.7	35.6	69.0	92.7	63.9	80.3

Table 11: Comparison of GCB and FLIP-opt against all noisy training mitigation on CIFAR. We use 3% poison rate in FLIP-opt to ensure high ASR. Some defense methods (e.g., SPL) can neutralize FLIP-opt but remain ineffective against our GCB attack.

can have good resilience to most of the defense methods. However, new-emerging defenses, especially clean-data-based defenses, are effective in defending our attacks.

GCB's Resilience on CIFAR-100

As shown in Table 14, our method shows the highest effectiveness against all the testing defenses except DBD. The ASR reaches best under defenses like AC (Activation Clustering) and ABL (Anti-Backdoor Learning). For the other methods, the ASR decreases a little but is still effective. This once again confirms that only self-supervised learning-based defenses like DBD (Decoupling-based Backdoor Defense) can effectively defend against our attack because our poisoned labels are totally unused in self-supervised learning.

Dataset↓	Corruption→ Attack↓	No Defense		JPEG		Smoothing		Color Shift		Color Shrink		Affine		Average
		ACC	ASR	ACC	ASR	ACC	ASR	ACC	ASR	ACC	ASR	ACC	ASR	
CIFAR-10	BadNet	93.2	73.8	79.1	50.8	39.9	3.3	81.9	53.1	85.4	40.7	79.7	49.8	45.2
	Blend	93.7	94.1	79.0	66.3	42.6	2.6	86.3	86.9	86.1	85.5	86.4	82.3	69.6
	BPP	91.9	76.4	81.7	2.0	47.1	2.0	84.9	78.9	41.7	74.8	88.6	84.3	53.1
	IA	90.5	79.6	75.3	7.2	33.0	2.6	78.7	75.1	81.4	83.8	86.5	65.9	52.4
	LF	93.5	86.1	79.6	86.7	39.5	88.0	85.3	78.2	86.2	78.2	81.6	89.5	84.5
	SIG	93.7	80.4	79.8	89.8	43.9	70.1	86.8	74.3	86.1	66.0	85.9	60.0	73.5
	SSBA	93.4	99.7	78.9	1.7	37.4	18.5	86.2	94.2	81.6	94.4	88.5	87.9	66.1
	WaNet	91.1	72.0	60.4	50.6	17.9	58.7	84.6	60.0	83.1	1.2	88.0	19.8	43.7
	FLIP	91.9	86.3	72.5	86.9	35.9	9.3	83.7	83.8	82.3	67.3	78.8	72.1	67.6
	GCB (ours)	92.6	100.0	77.6	100.0	40.7	100.0	84.4	98.4	84.9	100.0	84.2	100.0	99.7
CIFAR-100	BadNets	70.7	35.6	56.3	33.5	70.2	31.7	63.6	23.0	66.2	4.0	67.7	20.1	24.7
	Blended	70.9	91.5	56.2	72.0	70.5	90.1	64.2	84.5	65.5	59.7	68.5	86.6	80.7
	BPP	65.0	66.1	56.7	0.1	64.6	42.5	59.2	71.1	63.6	62.7	62.8	0.5	40.5
	IA	65.3	78.8	50.0	60.3	64.5	78.5	57.1	85.2	59.2	87.5	63.7	77.2	77.9
	LF	70.0	38.9	55.8	54.1	69.9	37.5	63.9	33.5	66.1	3.2	66.1	37.8	34.2
	SIG	70.4	77.7	53.5	80.9	24.1	91.5	64.3	67.3	65.6	13.7	64.9	91.1	70.4
	SSBA	70.7	98.8	52.7	4.0	24.6	90.6	64.6	91.8	65.1	4.0	61.2	97.2	64.4
	WaNet	63.7	92.7	38.7	77.4	2.0	98.3	58.5	82.9	60.8	0.1	13.1	97.7	74.9
	GCB (ours)	70.1	96.7	57.4	96.7	25.3	67.1	63.7	95.7	30.4	72.8	54.2	86.1	85.9

Table 12: Comparison of different attack methods against common image corruptions.

Defense→	DeepSweep (Qiu et al. 2021)		BNP (Zheng et al. 2022)		MCR (Zhao et al. 2020)		NPD (Zhu et al. 2024)		FT-SAM (Zhu et al. 2023)		SAU (Wei et al. 2024)		PGBD (Amula et al. 2025)		Avg.
	CA	ASR	CA	ASR	CA	ASR	CA	ASR	CA	ASR	CA	ASR	CA	ASR	
BadNet	85.3	1.9	93.2	15.2	90.5	2.0	91.1	0.9	92.8	1.7	90.6	2.2	90.7	0.7	3.5
Blended	70.9	65.5	93.8	93.0	91.4	41.7	91.5	74.2	93.2	51.8	91.2	32.2	87.1	24.3	54.7
SIG	84.5	41.6	93.7	80.6	90.9	31.8	91.3	63.6	92.9	49.5	85.8	0.8	86.8	0.5	38.3
IA	87.6	75.9	90.6	79.2	93.4	80.7	85.5	2.6	93.4	5.4	91.2	2.8	89.6	2.6	35.6
SSBA	71.8	81.2	93.3	99.7	90.8	39.3	91.2	8.8	92.8	60.3	86.7	2.6	88.4	5.2	42.4
WaNet	92.6	4.7	55.5	12.8	93.4	1.7	90.9	0.9	93.5	0.9	90.9	0.6	88.7	2.4	3.4
BPP	90.0	32.5	91.4	79.6	93.5	83.9	53.0	0.0	93.7	49.0	91.6	4.4	87.3	6.7	36.6
FLIP	70.7	26.9	92.0	85.9	90.2	0.4	90.1	0.0	93.0	0.5	91.2	0.5	84.1	10.8	17.9
GCB (ours)	77.9	93.2	92.3	100.0	90.8	78.0	90.6	97.4	92.7	1.8	90.6	5.4	85.5	21.1	56.7

Table 13: Comparison of different attack methods against **clean-data-based** defenses on CIFAR-10 with 2500 (5%) clean image-label pairs.

Defense→	AC		SS		ABL		DBD		CLP		EP		Avg.
	CA	ASR	CA	ASR	CA	ASR	CA	ASR	CA	ASR	CA	ASR	
BadNets	60.4	36.5	66.6	42.2	46.7	0.8	61.0	0.2	61.8	23.5	66.7	24.2	21.2
Blended	60.2	81.7	67.7	91.1	49.9	0.0	61.5	97.3	63.0	52.0	66.8	82.7	67.5
SIG	61.0	72.1	65.8	71.3	51.4	0.0	62.4	92.2	65.9	81.3	67.8	78.3	65.9
IA	60.6	63.3	67.0	69.1	61.1	63.3	61.7	0.1	64.2	1.1	62.7	0.6	32.9
LF	60.8	35.5	66.4	45.6	61.5	4.6	60.9	0.4	69.0	29.0	66.6	47.0	27.0
SSBA	61.1	94.5	67.1	98.5	50.9	0.0	62.0	0.4	69.9	99.2	68.6	98.9	65.2
WaNet	59.9	4.5	66.7	10.0	56.8	4.7	63.3	0.2	62.2	1.2	61.8	16.0	6.1
BPP	60.3	6.2	67.1	24.8	53.2	13.5	60.5	0.2	59.4	0.2	62.8	0.1	7.5
GCB (ours)	60.3	95.2	67.1	97.6	60.1	96.2	62.1	1.3	68.4	95.9	65.9	94.3	80.1

Table 14: Comparison of different attack methods against other defenses on CIFAR-100.



Figure 16: Image samples from different datasets. From top to bottom are ColorCIFAR10, VOC2012, CelebA respectively. The selected training images are unmodified, representing a subset of clean images.

GCB’s Resilience compared with FLIP on Noisy training mitigation.

GCB demonstrates substantially higher resilience against noisy training mitigation techniques compared to FLIP-opt, as shown in Table 11. While several noise-robust methods such as SPL and BootStrap significantly reduce FLIP-opt’s attack success rate (ASR), they fail to mitigate GCB’s effectiveness, which consistently maintains a near-100% ASR across all defenses. Moreover, GCB preserves competitive CA, often outperforming FLIP-opt even under strong defenses. This indicates that GCB’s gradient-consistent backdoor mechanism is more robust to label noise and regularization-based filtering, allowing it to persist where traditional feature-aligned poisoning (e.g., FLIP-opt) is largely neutralized.

Additional Ablation Study on Irrelevance

In this section, we provide further clarification and empirical evidence to demonstrate the irrelevance between the trigger condition c and the benign classification task $y | x$. Specifically, we investigate whether the introduction of the trigger affects the classification accuracy of clean images when predicting their ground truth labels.

Verification of Irrelevance: To assess the irrelevance, we compare the classification accuracy of clean images with that of triggered images under the ground truth labels. Formally, we evaluate $P(y | x)$ and $P(y | x, c)$. As illustrated in Fig. 17. Similarity between these probabilities indicates that the trigger does not interfere with the benign classification task, thereby satisfying the irrelevance condition.

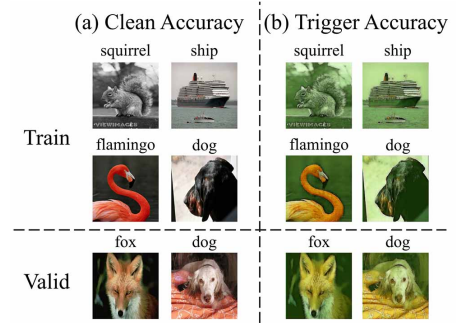


Figure 17: Metric design for irrelevancy: The closer the Triggered Accuracy (TA) is to the Clean Accuracy (CA), the higher the irrelevance between the generated images and the benign features.

Experimental Design:

1. **Clean Accuracy (CA):** Measures the accuracy of classifying clean images x to their ground truth labels y , denoted as $P(y | x, c = 0)$.
2. **Triggered Accuracy (TA):** Measures the accuracy of classifying triggered images x' to their ground truth labels y , denoted as $P(y | x, c = 1)$.

We conducted experiments by adding triggers to all images in both the training and testing datasets while preserving the original labels. Models with the same architecture as those used in the benign setting were trained, and each experiment was replicated five times to ensure statistical significance.

	CIFAR-10	CIFAR-100
CA	93.9%	71.0%
TA without LC	14.3%	3.8%
TA (Our Method)	91.2%	67.4%

Table 15: Performance on CIFAR-10 and CIFAR-100 Datasets. TA drops significantly without LC, which means triggered images can not be recovered to their original labels, indicating a possible modal collapse.

The results presented in Table 15 indicate that **without label conditioning (LC)**, the triggered accuracy (TA) decreases significantly, suggesting that the trigger interferes with the benign classification task and violates the irrelevance condition. In contrast, with label conditioning, the TA remains comparable to the CA, which confirms that our method maintains irrelevance between the trigger and the benign task.

Upon further examination of images without Label Conditioning (LC), we observed a collapse into patterns resembling a single class, akin to mode collapse commonly observed in Generative Adversarial Networks (GANs). This phenomenon leads to the markedly low TA observed. As illustrated in Fig. 18, all triggered images collapse into a single pattern. Although these collapsed patterns can still exhibit high ASR in attacks because they retain similar features to the selected training images, their irrelevance scores are very low.



Figure 18: One example of our GCB without Label Condition (LC). All triggers collapse into one pattern. This can still achieve a high ASR but results in a very low irrelevance score.

GCB’s Resilience to Abnormal Sample Detection.

Since the trigger of GCB is GAN-generated, there may be a significant distributional gap between the generated trigger and real image data. Consequently, it is essential to analyze the method’s resistance to defense strategies based on abnormal sample detection. Specifically, we employ Uniform Manifold Approximation and Projection (UMAP) to visualize the distribution of intermediate features in the victim model, a standard approach in backdoor detection research (Qi et al. 2022; Wu et al. 2024). We investigate two key aspects:

Detectability of Poisoned Training Samples

We assess whether poisoned training samples can be detected as outliers when compared to clean samples. By visualizing the feature distributions of poisoned and clean samples using UMAP, we find that the poisoned samples generated by our method exhibit a distribution highly consistent with that of clean images. As shown in Figure 19, the poisoned samples are indistinguishable from clean samples in the feature space of the victim model.

The primary reason for this indistinguishability is that our GAN-based trigger generator produces poisoned samples that carry subtle and natural-looking modifications. These modifications result in poisoned features that are in-distribution, making them difficult to separate using UMAP. This characteristic outperforms existing backdoor methods in evading detection. Similar observations have been reported in previous studies (Qi et al. 2022).

Detectability of Triggered Test Samples

We also evaluate whether triggered test samples can be detected as outliers during inference. By applying our GAN-based triggers to test samples and analyzing their feature distributions across various neural network layers, we observe that the triggered samples align closely with the distribution of clean images. Figure 19 illustrates that the triggered test samples are embedded in the same manifold as clean samples at different layers of the network.

The GAN framework ensures that the triggers mimic the real image distribution, effectively evading anomaly detection methods that rely on distributional differences. The triggered test samples exhibit similar distributions to poisoned training samples across all examined layers, making simple outlier detection infeasible in such cases.

Impact of Network Layers on UMAP Visualization

We further explore the impact of different network layers on the UMAP visualization of our method. As shown in Figure 20, we visualize the feature distributions at various layers (e.g., Layer1, Layer2, Layer3, Layer4) of the PreActResNet-18 model. In all cases, both poisoned training samples and triggered test samples exhibit in-distribution properties similar to clean samples. This consistent behavior across layers reinforces the challenge of detecting our method using simple outlier detection techniques.

Hyperparameter Analysis

To validate the hyperparameter sensitivity of our method, we conducted experiments on two key parameters: the learning rate and the weight factor of the information loss λ . These two terms are also considered crucial in the original InfoGAN paper (Chen et al. 2016). We evaluated the training outcomes based on three aspects: (1) ASR, (2) visualization of triggered test images, and (3) visualization of selected training images.

(a) Effect of Learning Rate We tested five different learning rates: 1×10^{-5} , 3×10^{-5} , 1×10^{-4} , 3×10^{-4} , and 1×10^{-3} . We found that the ASR remained high (over 90%) across all learning rates. However, when the learning rate was very low or very high (1×10^{-5} or 1×10^{-3}), strong artifacts were observed in the triggered test images, making these samples easier to detect at test time. Interestingly, we also found that different learning rates sometimes converged to different trigger patterns. At a learning rate of 3×10^{-4} , the trigger became a frame around the image, while other learning rates resulted in triggers with special colors. This finding—that different learning rates result in different patterns—was also observed in the original InfoGAN (Chen et al. 2016).

(b) Effect of Weight Factor λ We tested five values for the weight of the information loss λ : 0.05, 0.1, 0.25, 0.5, and 1.0. We observed that the ASR dropped significantly at lower weights (0.05 and 0.1). This is because when the weight is very small, the network focuses less on identifying whether an image contains a trigger, making the trigger pattern less prominent and harder to learn. Conversely, when the weight is very high, the discriminator focuses too much on identifying whether an image has a trigger, neglecting the realism of the generated images. This results in images with noticeable artifacts and a large distribution gap between real and fake images.

In conclusion, both the learning rate and the weight factor λ are robust within a certain range. However, when these parameters become too high or too low, their effects differ. The learning rate affects the amount of artifacts in the generated images but does not significantly impact the ASR. On the other hand, the weight factor λ has a large impact on the ASR.

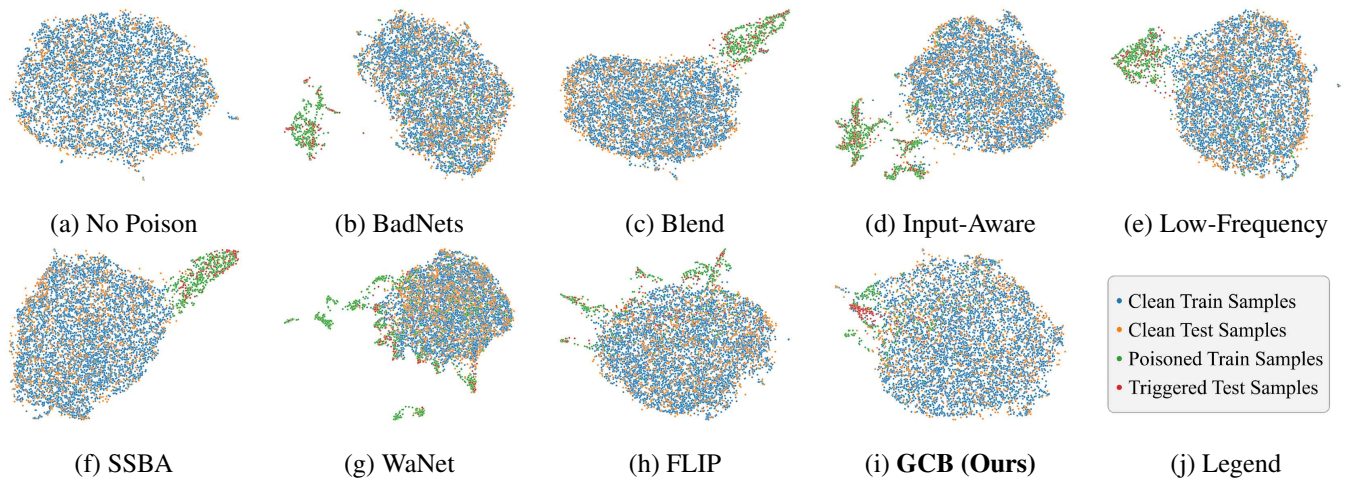


Figure 19: UMAP Visualization of different backdoor attack methods in the CIFAR-10 dataset.

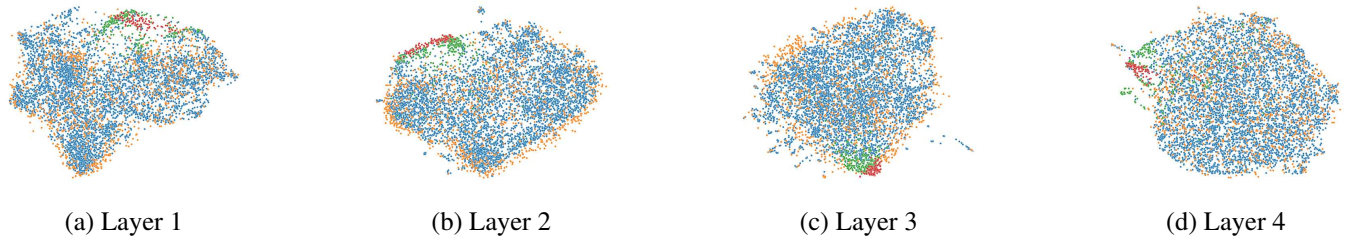


Figure 20: UMAP Visualization of different layers on PreActResNet in GCB.

Learning Rate	1e-5	3e-5	1e-4	3e-4	1e-3
Metrics					
Triggered Test Images					
Selected Train Images					
ASR	96.3%	100%	100%	91.6%	98.4%

Figure 21: Effect of learning rate on the trigger patterns and artifacts in the generated images. Each column corresponds to a different learning rate.

Loss Weight λ	0.05	0.1	0.25	0.5	1
Metrics					
Triggered Test Images					
Selected Train Images					
ASR	66.1%	97.3%	100%	94.5%	13.2%

Figure 22: Effect of the information loss weight factor λ on ASR and image quality. Each column corresponds to a different value of λ .